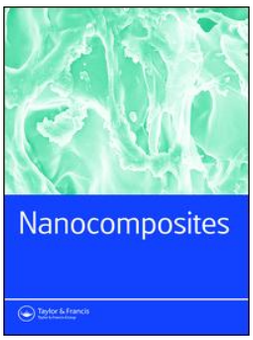

Nanocomposites

ISSN: 2055-0324 (Print) 2055-0332 (Online) Journal homepage: http://www.tandfonline.com/loi/ynan20

Thermally activated shape memory behavior of copolymers based on ethylene reinforced with silica nanoparticles

Valentina Sessini, David Brox, Antonio Julio López, Alejandro Ureña & Laura Peponi

To cite this article: Valentina Sessini, David Brox, Antonio Julio López, Alejandro Ureña & Laura Peponi (2018): Thermally activated shape memory behavior of copolymers based on ethylene reinforced with silica nanoparticles, Nanocomposites, DOI: 10.1080/20550324.2018.1472723

To link to this article: https://doi.org/10.1080/20550324.2018.1472723

Published online: 18 Jun 2018.

NANOCOMPOSITES, 2018
https://doi.org/10.1080/20550324.2018.1472723

Taylor & Francis
Taylor & Francis Group

RESEARCH ARTICLE

OPEN ACCESS Check for updates

Thermally activated shape memory behavior of copolymers based on ethylene reinforced with silica nanoparticles

Valentina Sessini[a], David Brox[a,b], Antonio Julio López[b], Alejandro Ureña[b] and Laura Peponi[a]

[a]Instituto de Ciencia y Tecnología de Polímeros, ICTP-CSIC, Madrid, España; [b]Departamento de Matemática Aplicada, Ciencia e Ingeniería de Materiales y Tecnología Electrónica, Escuela Superior de Ciencias Experimentales y Tecnología, Universidad Rey Juan Carlos, Móstoles, España

ABSTRACT

In this work, a study on the dual-shape and triple-shape memory response of poly(ethylene-co-methacrylic acid) copolymer, EMAA, and its counterpart neutralized with sodium salt, EMAA-Na has been report. Moreover, both matrices were reinforced with silica nanoparticles in different amount. Morphological, thermal and mechanical properties were studied confirming the good dispersion of the nanoparticles into both polymeric matrices. The addition of silica nanoparticles increases the mechanical response of both polymeric matrices without affecting their shape memory response leading to a possible increasing use of both polymers in the industry. Moreover, the ionomeric polymer reinforced with 1 wt.% silica nanoparticles present excellent thermally activated triple-shape memory response.

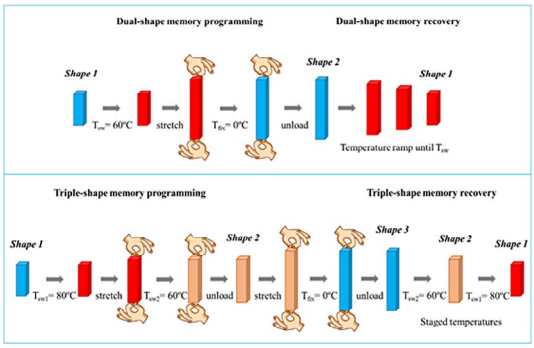

ARTICLE HISTORY
Received 6 March 2018
Accepted 23 April 2018

KEYWORDS
Shape memory; ionomers; ethylene copolymers; Silicon Dioxide nanoparticles; nanocomposites, methacrylic acid

Introduction

Shape memory polymers (SMPs) are a class of smart materials with the capability to change their shape when an external stimulus is applied, such as temperature [1–3], humidity [4,5], pH [6], light [7] or an electric field [8] by fixing a temporary shape. Moreover, they are able to recover their original shape when the external stimulus is applied again. Shape memory behavior is not an intrinsic property of the material, therefore an adequate phase morphology is required [9,10]. The presence of a dual domain in the polymer, i.e. permanent network and reversible/switching domains is necessary to designing SMPs. In this type of polymers, the switching domains are responsible for the temporary shape of the material, which is programmed during the 'programming stage'. On the other hand, the permanent network is responsible for the retention of the original shape, memorizing the initial shape during the 'recovery stage'. A unique classification of the applied stimuli does not exist; however, they can be classified as direct stimuli such as temperature and light, and non-direct ones. The direct ones can be applied in both stages, to fix the temporary shape and to recover the original one, programming and recovery respectively [11]. Meanwhile, non-direct stimuli only act in the recovery stage, i.e. electric and magnetic fields, pH or humidity stimuli, needing the help of temperature as external stimulus, in the programming stage [12]. Therefore, it is understandable why, in general, thermally activated shape memory polymers are the most studied SMPs. In heating-responsive SMPs, the switching domains are associated to a transition temperature (T_{trans}). This temperature can be the glass transition temperature (T_g) or the melting temperature of the polymer (T_m) depending on the amorphous or crystalline nature of the switching phase. During the programming stage, the sample is heated to a temperature above T_{trans}

CONTACT Laura Peponi lpeponi@ictp.csic.es

and subsequently a deformation is applied. Cooling down the temperature below T_{trans}, the temporary shape is fixed and the applied stress to deform the sample is realized. The application of a temperature above T_{trans} enables the recovery of the original shape.

The above-mentioned SMPs are the most common ones and they are usually referred as 'one-way shape memory polymers,' with two active phases – i.e. the permanent network and switching domain – and an external stimulus to trigger the phases in order to change from one shape to another. This kind of SMPs is also called 'dual-shape memory polymers,' because a permanent shape is transformed into a temporal one. However, depending on the morphology and on the proprieties of a specific SMP, it is possible to program two or more temporary shapes. These materials are known as 'triple-shape memory polymer' or 'multiple-shape memory polymers,' respectively [13,14]. In general, a material with 'n'-shape memory response, presents 'n-1' temporary shape [12]. Triple-shape memory polymers need one programming stage, in which both temporary shapes are programmed, and the application of two different triggers to firstly recover the intermediate temporary shape and subsequently recovering the original shape. Triple-shape memory effect was first introduced by Lendlein et al. in 2006 [15] showing the possible application fields of SMPs such as biomedical devices, actuators, and smart adhesives.

In the literature, there are numerous polymeric systems able to act as SMPs including physically crosslinked thermoplastics, blends, and composites [16–18]. Between them, ionomers are ion-containing polymers with a maximum ionic content of ca. 15 mol % [19]. Polyolefin ionomers are produced by copolymerization or post-polymerization modification to introduce carboxylate or sulfonate functional groups followed by neutralization to produce metal counter-ions (e.g. Na^{+}, K^{+}, Mg^{+2}, Ca^{+2}, Zn^{+2}, Al^{+3}) [19]. In these ionomers, strong thermodynamic immiscibility between the polymer backbone and the ionic groups as well as strong interactions by columbic potentials between the ionic charges, lead to a microphase separation and to the formation of dispersed ionic aggregates called ionic clusters, which physically crosslink the polymer [20]. In many systems these physical crosslinks can persist to high temperatures (>150 °C) as reported in literature [21], therefore they can be used as the permanent network in SMPs.

Poly(ethylene-co-methacrylic acid) copolymer, EMAA, neutralized with sodium salt is a well-known ionomer with the tradename of Surlyn® manufactured by Dupont™ Company. The self-healing properties of this polymer under high speed impact, i.e. ballistic damage [22,23], and even under hyper-velocity impacts (1–4 km/s) simulating space debris impacts [24] has been studied. Its two physical networks formed by ionic clusters, thanks to ionic bonds, and the ethylene crystals enabled the shape memory behavior of these materials. The broad melting point for the ethylene crystals provides the opportunity for multi-shape memory behavior as reported in literature for poly(ethylene-co-methacrylic acid) copolymer neutralized with zinc [21,25]. Recently, Zhao et al. [26] demonstrated shape memory behavior of 3D printed objects using the same commercially available zinc neutralized poly(ethylene-co-methacrylic acid) without any new chemistry requirements. On the other hands, Lu et al. [27] in 2016 reported that commercial Surlyn® 8940, neutralized with sodium, exhibits both one-way multi-shape memory effects and tunable two-way reversible actuation.

However, nowadays, a very important challenge is to study shape memory nanocomposite materials (SMCs) [28], thus taking into account that the incorporation on nanoparticles to the polymeric matrix can strongly affect its shape memory behavior by changing its transition temperature [17]. In general, nanomaterials can be considered as excellent reinforcements for polymeric matrices with the ability to enhance the performance of final polymer nanocomposites [29].

The use of carbon-based nanofillers, i.e. single-walled carbon nanotubes (SWCNTs) [30,31] or multi-walled carbon nanotubes (MWCNTs) [32] can convert the electrical current, externally applied, into heat through a Joule effect, triggering the SMPs behavior. Furthermore, the external application of microwaves to a SMCs reinforced with MWCNTs can thermally induce the SMCs shape recovery [33]. Noble metal nanoparticles such as silver [34] or gold [35] have been also studied due to their photo-thermal effect, the ability to transform the deep UV – near IR wavelength light into heat energy. Oxide metal nanofiller, such as Fe_3O_4 has been added to SMP matrix to remotely trigger, using an external magnetic field, the change between the temporary shape and the permanent one, with possible applications to activate an object within the body, but preserving the heating of the human tissue [36,37]. Recently, Odent et al. [38] reported an interesting study on shape memory nanocomposites based on poly(lactic acid) reinforced with silica nanoparticles by forming ionic hybrids. Moreover, silica nanoparticles have been previously studied to improve the mechanical properties of epoxy resins [39]. Furthermore, the good compatibility with the polymer matrix [40,41] due to the hydrogen bonding of the silica nanoparticles increases the mechanical properties of the matrix [42].

In the present work, silica nanoparticles have been used in different proportions as nanofillers for the EMAA copolymer. In particular, the main goal of this work is to improve the poor mechanical properties of the ionomer Surlyn® resin and its precursor, Nucrel®, without hindering their shape memory behavior. Thus, the morphological, thermal, and mechanical properties of EMAA copolymer and ionomer-based materials were studied in this work as well as their shape memory behavior. In particular, the improvement of their mechanical response can deal

to an increasing use of both polymers in the industry. Moreover, a triple shape-memory response of the Surlyn® reinforced with 1 wt % nanosilica has been obtained.

Materials and methods

Materials

Commercial poly(ethylen-co-methacrylic acid) random copolymer (EMAA) named Nucrel® 960 (contained 15 wt.% of methacrylic acid (MAA) comonomer) and its ionomer, Surlyn® 8940, with 30% of MAA comonomer neutralized by sodium (EMAA-Na), were kindly provided by Dupont™ Company.

Silicon Dioxide Nanopowder (SiO_2) with a particle average size of 7–14 nm and specific surface higher than 200 m^2/g was supplied by EMFUTUR.

Melt-processing of the nanocomposites

Three different nanocomposites were prepared using both, Nucrel® as well as Surlyn®, with different amount of SiO_2 nanoparticles, i.e. 0.5, 1, and 3 wt.%.

Before their processing, the polymers and the nanofiller were dried at 60 °C for 48 h. The nanocomposites were melt-processed by a microextruder equipped with twin conical co-rotating screws (MiniLab Haake Rheomex CTW5, Thermo Scientific, capacity 7 cm^3) with a screw rotation rate of 130 rpm, temperature of 150 °C, and residence time of 5 min. The processed nanocomposites were named empathizing the SiO_2 nanoparticles amount present in the respective polymer matrix, such as NU0SiO_2, NU0.5SiO_2, NU1SiO_2, and NU3SiO_2 indicating the presence of 0, 0.5, 1, and 3 wt.% of SiO_2 nanoparticles on the Nucrel® matrix. The same nomenclature was used for the nanocomposites based on Surlyn®, SU0SiO_2, SU0.5SiO_2, SU1SiO_2, and SU3SiO_2. The extruded nanocomposites were successively thermo-compressed in a Dr Collin 200 × 200 mm press at 160 °C and 50 bars in order to obtain films to carry out their characterization.

Characterization methods

Field Emission Scanning Electron Microscope (FE-SEM, Hitachi S8000) in transmission mode was used to observe the SiO_2 nanoparticles dispersion into the polymeric matrix in the nanocomposites. In order to study the morphology of the pristine nanoparticles a dispersion of SiO_2 in water was prepared and 1 drop was placed on a square mesh copper grid. After water evaporation, the grid was analyzed. Regarding the study of the SiO_2 dispersion in the polymeric matrix, ultrathin sections were made at 50–70 nm by ultramicrotome, using a diamond knife and placed on the square mesh copper grid.

The thermal properties were investigated by Differential Scanning Calorimetry (DSC) analysis. The dynamic DSC measurements were performed in a Mettler Toledo DSC822e instrument, under nitrogen flow (30 ml/min). Samples of about 10 mg were sealed in aluminum pans. Thermal cycles were composed by the following 'heat/cool/heat' procedure: heating at 10 °C min^{-1} from 0 to 150 °C, cooling at 10 °C min^{-1} to 0 °C and heating again at 10 °C min^{-1} to 150 °C. The first heating scan was normally used to erase prior thermal history of the samples and in our case, we use it to study the thermal behavior of the materials as obtained after their processing to establish the right parameters for the thermo-mechanical cycles, obtaining the values for the melting temperatures (T_m), and the melting enthalpy (ΔH_m). From the cooling scan, the crystallization temperature (T_c) was obtained. The degree of crystallinity (X_c) of each sample was calculated, according with the equation below:

$$\chi_c(\%) = \left(\frac{\Delta H_m}{\Delta H_m^{100}}\right) \times 100 \quad (1)$$

where ΔH_m^{100} is the specific melting enthalpy for a 100% crystalline PE (278 J/g) [43].

Dynamic Mechanical Thermal Analisys (DMTA) of the samples was carried out using a DMA Q800 from TA Instrument in film tension mode with an amplitude of 5 μm, a frequency of 1 Hz, a force track of 125%, and a heating rate of 2 °C min^{-1}. The relaxation temperatures are defined at the loss modulus profiles. Samples subjected to DMA were cut from compression-molded films into regular specimens of approximately 20 mm × 5 mm × 0.50 mm.

Thermogravimetric analysis (TGA) was carried out using a TGA Q500 thermal analyzer from TA Instrument. Neat polymers and their nanocomposites were analyzed by dynamic mode using about 10 milligrams of sample from room temperature to 800 °C at 10 °C min^{-1} under nitrogen atmosphere with a flow of 60 mL min^{-1}. Temperatures at the maximum degradation rate (T_{max}) were calculated from the first derivative of the TGA curves (DTG) and the initial degradation temperatures were toked at 5% of weight loss.

Mechanical properties were determined using an Instron Universal Testing Machine at a strain rate of 150 mm min^{-1}. Tensile test measurements were performed on 5 dog-bone specimens with a width of 2 mm, thickness of 0.50 mm and leaving an initial length between the clamps of 20 mm. From these experiments were obtained the elastic modulus, as the slope of the curve between 0 and 2% of deformation, the elongation at break and the maximum stress reached.

Thermally activated shape memory characterization

Thermally activated shape memory properties were studied using a stress-controlled DMA Q800 from TA Instruments in film tension mode. Samples for the

thermo-mechanical cycles were cut from compression-molded films into rectangular specimens of approximately 20 mm × 5 mm × 0.50 mm. Dual-shape memory experiments are conducted according to the thermo-mechanical cycle showed in Figure 1(a). The samples were heated at the switching temperature (T_{sw}) for 5 min, following by a stress-controlled uniaxial stretching applied until a fixed percentage of deformation, i.e. 50%. They were then quenched at 0 °C (T_{fix}) under the same constant stress, which after 10 min was released. A free-strain recovery is then performed under continuous heating conditions at 3 °C min^{-1} until the selected T_{sw}.

Triple-shape memory experiments were also carried out using a stress-controlled DMA Q800 from TA Instruments in film tension mode and they were conducted according to the scheme in Figure 1(b). Typical triple-shape memory thermo-mechanical cycles involve 2 different temporary shapes as well as two different T_{sw}. In our case, samples were heated at the T_{sw1} for 5 min and were uniaxial stretched under controlled stress until 40% of deformation. After that, the samples were quenched for 10 min at the T_{sw2} followed by stress unload for 10 min, fixing shape 2. In order to program the third shape, a stress-controlled uniaxial stretching was applied at the same temperature, until 80% of deformation. After quenching at the T_{fix} under the same constant stress for 10 min the stress was removed again and a free-strain recovery was finally performed at staged switching temperatures, T_{sw2} and T_{sw1} respectively, heating at 3 °C min^{-1}.

Therefore, with the aim to get a quantitative estimation of the shape memory properties of the material, the strain fixity ratio (R_f) and the strain recovery ratio (R_r) have been calculated. In particular, R_r, the ability to recover the initial shape, was taken as the ratio of the recovered strain to the total strain, as given by the following equation:

$$R_r(N) = \frac{\left(\varepsilon_m - \varepsilon_p(N)\right)}{\varepsilon_m - \varepsilon_p(N-1)} \times 100\% \quad (2)$$

R_f, the ability to fix the temporary shape, was taken as the ratio of the fixed strain to the total strain, as presented by the Equation (3):

$$R_f(N) = \frac{\varepsilon_u(N)}{\varepsilon_m} \times 100\% \quad (3)$$

where, ε_m is the deformed strain, ε_u the fixed strain, ε_p the recovered strain and N is the number of cycles.

Results and discussion

The dispersion of SiO_2 nanoparticle into the polymeric matrix was observed by FE-SEM analysis in transmission mode. FE-SEM images of the SiO_2 nanoparticles dispersed in water at different magnifications are showed in Figure 2(a) and (b), confirming the particle average size of about 10 nm.

In Figure 3 the FE-SEM images of the cross-section of SiO_2-reinforced nanocomposites are showed. Figure 3(a) and (b) show images of the cross-section of nanocomposite based on Nucrel® reinforced with 1 and 3 wt.% SiO_2, respectively, as well as Figure 3(c) and (d) show the cross-section of nanocomposites based on

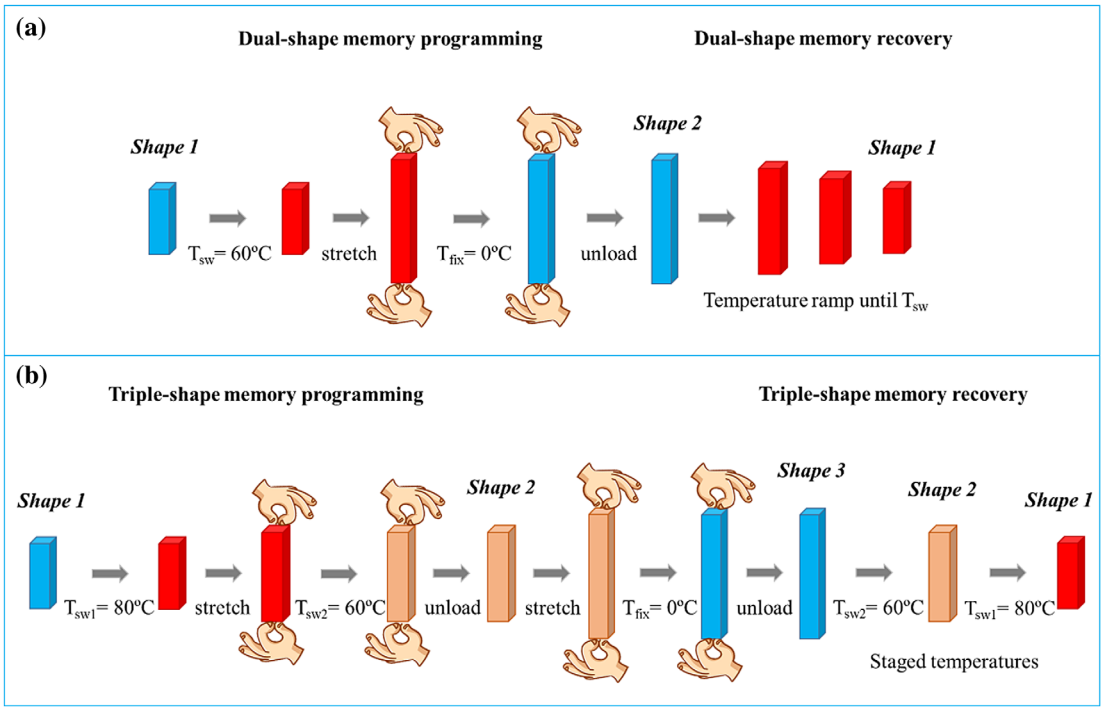

Figure 1. Schematic description of: (a) a dual-shape memory cycle and (b) a triple-shape memory cycle.

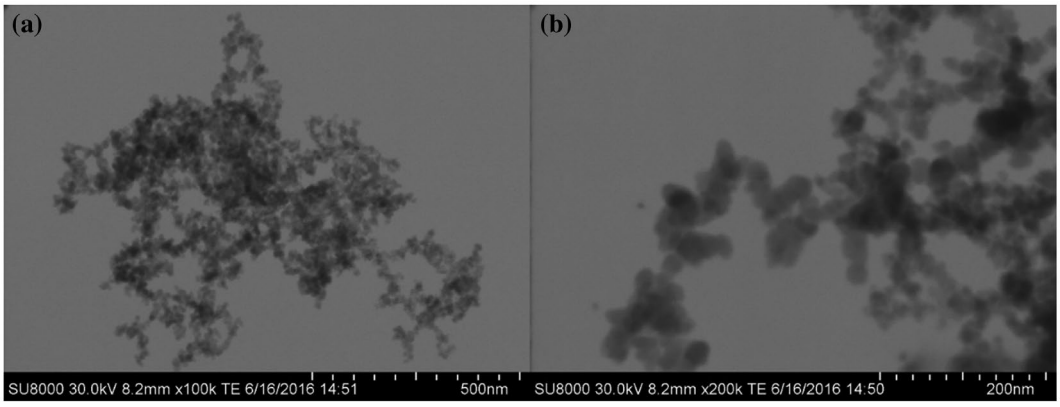

Figure 2. FE-SEM images of SiO_2 nanoparticles at different magnifications, (a) 100000× and (b) 200000×.

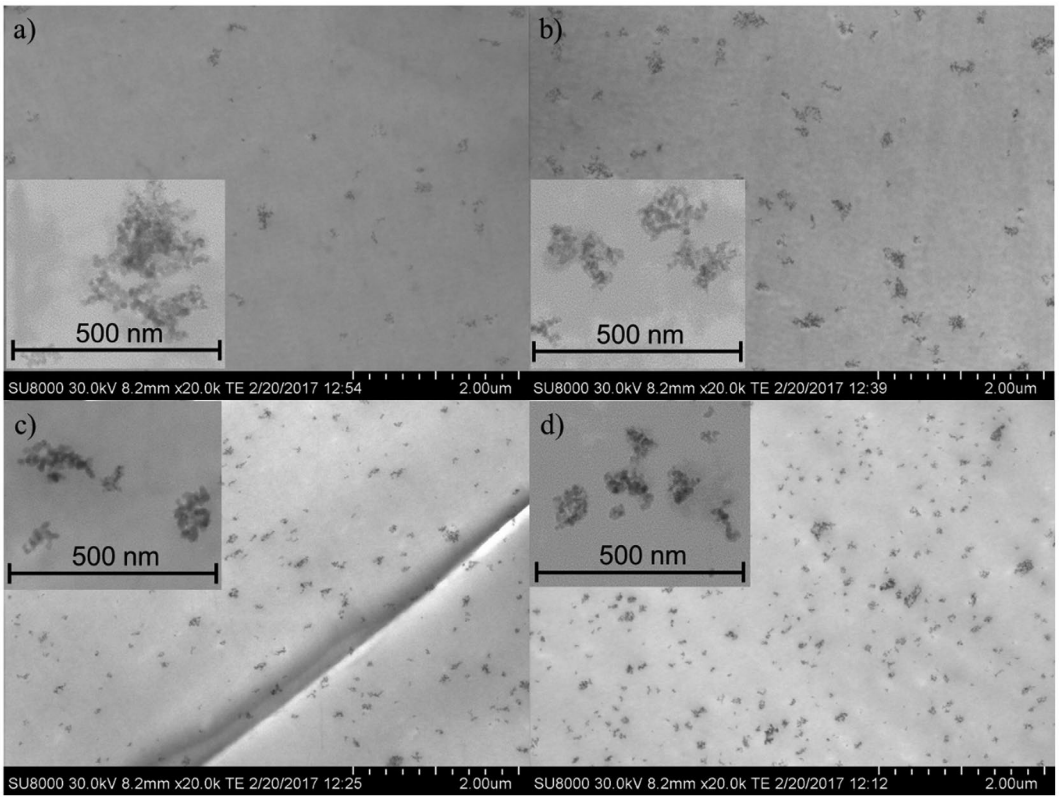

Figure 3. FE-SEM images of the cross-section of SiO_2-reinforced nanocomposites, (a) NU1SiO_2, (b) NU3SiO_2, (c) SU1SiO_2, and (d) SU3SiO_2.

Surlyn® reinforced with 1 and 3 wt.% SiO_2, respectively. A good dispersion of SiO_2 nanoparticles was observed for all the EMAA-based nanocomposites although an improvement of the dispersion was noticed in the case of EMAA-Na nanocomposites probably due to the interactions between SiO_2 nanoparticles and the ionic charges present in the EMAA-Na ionomer. It should be highlighted that very small aggregates of SiO_2 are presented. However, they exhibit dimensions ranging from 100 to 300 nm, which are small enough to provide improved properties for the nanocomposites, as it was already reported for polyurethane nanocomposites reinforced with silica nanoparticles [42].

EMAA copolymers and their ionomer resins show a complex thermal and thermo-mechanical behavior due to their complex structure containing polyethylene (PE) crystals, amorphous polymer chains, and ionic aggregates, in the case of the ionomers [44,45].

The DSC thermograms for all the processed samples are shown in Figure 4. As can be observed in the first heating scan (Figure 4(a) and (d)), EMAA-based samples exhibited two endothermal peaks. The highest temperature peak in the thermograms clearly corresponds to the melting temperature of polyethylene crystals while for the lowest temperature peak different and controversial explanations are given in literature.

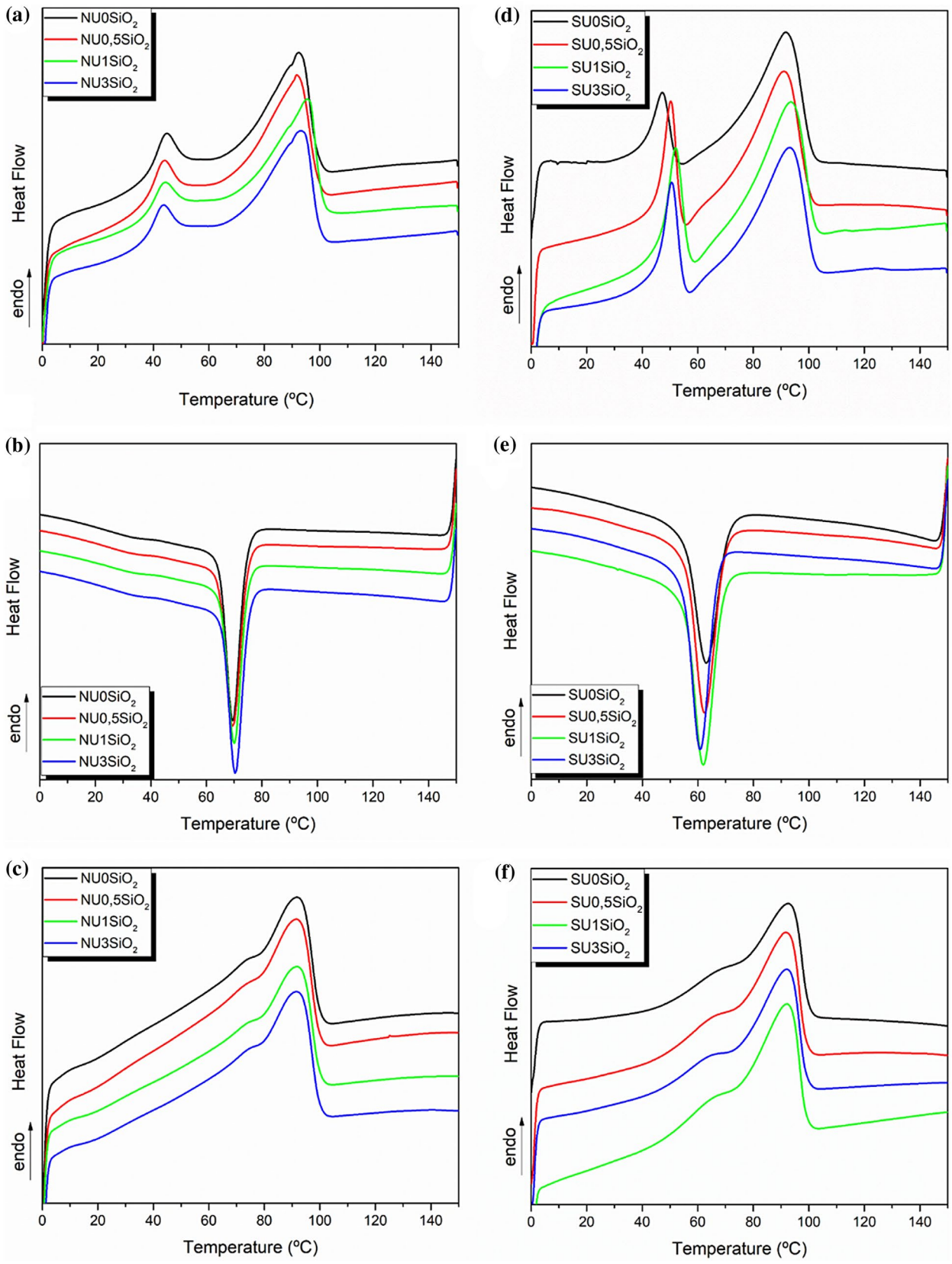

Figure 4. Heating–cooling–heating scans of DSC analyses for all the processed EMAA based neat materials and their nanocomposites reinforced with SiO_2 nanoparticles: (a-b-c) neat EMAA and its nanocomposites and (d-e-f) neat EMAA-Na and its nanocomposites.

One of these explanations, first proposed by Marx and Cooper [46], ascribed the lower endothermic peak to the melting of small PE secondary crystals that slowly form following the primary crystallization. Many other publications followed the same model [21,45,47,48]. Dolog et al. [21] reported that this fact results from the annealing of the sample at room temperature, which is above their glass transition temperature. However, several other publications attribute this lower temperature peak to an order-disorder transition within the ionic

Table 1. Thermal properties of all the processed samples.

	DSC[a]					TGA	
Sample	T_{m2} (°C)	T_{m1} (°C)	T_c (°C)	ΔH_m (J/g)	X_c (%)	$T_{5\%}$ (°C)	T_{max} (°C)
$NU0SiO_2$	45	93	70	44	16	416	462
$NU0.5SiO_2$	45	92	70	47	17	415	464
$NU1SiO_2$	45	96	70	48	17	411	464
$NU3SiO_2$	44	93	70	44	16	412	459
$SU0SiO_2$	43	92	63	47	17	409	483
$SU0.5SiO_2$	50	91	63	46	17	418	481
$SU1SiO_2$	52	94	62	46	17	422	482
$SU3SiO_2$	51	93	61	50	18	419	479

[a]The values have been taken from the first heating scan excluding T_c values that have been taken from the cooling scan.

aggregates [27,49–52] although it is reported in literature that these aggregates persist to temperatures well above the melting of PE primary crystals in EMAA ionomers [45,53,54].

In this work we followed the model that ascribes the lower temperature endothermic peak to the PE secondary crystals, accordingly with our previous work [16].

Indeed, studying the thermal behavior of EMAA copolymer and its SiO_2-reinforced nanocomposites (Figure 4(a)) it is easy to notice that all the samples shown the lower endothermic peak even if they are not in their ionic form. In Figure 4(a) and (d) the primary crystals melt in the range between 60 and 105 °C with a maximum melting temperature around 90 °C for both EMAA and EMAA-Na series, as well as the small secondary crystals, which melt between 35 and 60 °C with a maximum melting temperature of 45 °C. The thermal properties of all the processed materials are summarized in Table 1. Observing the cooling (Figure 4(b) and (e)) and the second heating scans (Figure 4(c) and (f)), only one peak was detected in the thermograms, confirming that the formation of the secondary crystals depends on the time [55] as well as on the annealing conditions of the sample at room temperature. Furthermore, the broad melting region observed in the second heating scan for both series of materials, EMAA and EMAA-Na, indicates a broad distribution of crystallites size of PE.

A slight decrease of the crystallization temperature was observed by increasing the SiO_2 amount in the nanocomposites of EMAA-Na ionomer. At the same time, an increase of the PE secondary crystals T_m (T_{m2}), thus comparing neat $SU0SiO_2$ with its nanocomposites, is detected. SiO_2 nanoparticle does not significantly interfere with secondary and primary crystallization in both series of nanocomposites. This fact is probably due to their well-defined spherical nature that permits to be inserted without affecting the thermal properties of the materials. In general, we can conclude that the presence of the SiO_2 nanoparticles did not affect the thermal properties of all the processed materials. This result is supported by those reported in literature for Surlyn®/silicate hybrid materials obtained by sol–gel process [53].

The TGA and DTG thermograms are reported in Figure 5 for both EMAA and EMAA-Na series. Comparing the neat materials, $NU0SiO_2$ and $SU0SiO_2$, the appearance of a small holder in the main degradation peak was noticed for the ionomer resin, probably due to the presence of the neutralized MAA comonomer fraction. The thermal degradation properties, in terms of $T_{5\%}$ and T_{max}, are summarized in Table 1. No significant changes in the $T_{5\%}$ were observed for EMAA-based materials with the presence of SiO_2 particles while an increase of about 10 °C was determined for EMAA-Na materials. Regarding the T_{max}, a slightly increase was observed by increasing the SiO_2 amount, for $NU0.5SiO_2$ and $NU1SiO_2$, followed by a drop of the T_{max} for $NU3SiO_2$ throughout lower values compared with that of its neat counterpart. The same tendency was observed for $SU3SiO_2$ characterized by a T_{max} lower than 4 °C compared with $SU0SiO_2$.

Dynamic thermo-mechanical analysis was performed in order to study the main chain relaxation in the EMAA-based materials and their nanocomposites. The storage modulus, loss modulus and tanδ curves are reported in Figure 6 for EMAA copolymer and EMAA-Na ionomer as well as their SiO_2-reinforced nanocomposites. All EMAA-based materials have similar elastic properties. On the other hand, the EMAA copolymer exhibits a lower storage modulus compared with EMAA-Na ionomer. EMMA copolymer and its SiO_2 nanocomposites showed two main relaxations in the range of temperature between −140 and 100 °C. From the loss modulus curve (Figure 6(b)), it is possible to observe the first relaxation, at around −130 °C. In this work we refer to it as γ and it has been ascribed to a local molecular motion of the amorphous segment of PE [51]. Moreover, a second relaxation (β') was noticed at around −50 °C and it was assigned to a micro-Brownian segmental motion in the amorphous region, where carboxylic acid dimers act as crosslinks and restrict the motion [51,56]. β' relaxation is more evident for $NU1SiO_2$ probably due to the interaction between the carboxylic acid groups and the SiO_2 nanoparticles. Afterward, a broad peak centered at around 20 °C was assigned to the melting of the secondary crystal phase already observed in the DSC analysis. For EMAA ionomer resin and its nanocomposites, the same relaxations were observed but β' relaxation was shifted to lower temperatures, at about – 45 °C (β relaxation). Although various explanation have been proposed for this relaxation over the years, in this work it was ascribed to the ion-depleted in the amorphous region [57]. The peak corresponding to the T_{m2} was shifted to higher temperature for EMAA-Na ionomer and its nanocomposites compared with the EMAA copolymer. Indeed, this peak was even split in two for EMAA-Na ionomer indicating the contribution of two chain relaxations. PE secondary crystals melting occurred in the range between 0 and 60 °C but for EMAA-Na ionomer, it was overlapped by the α relaxation, ascribed to the devitrification of ion-reach regions, as it was previously reported in literature [16].

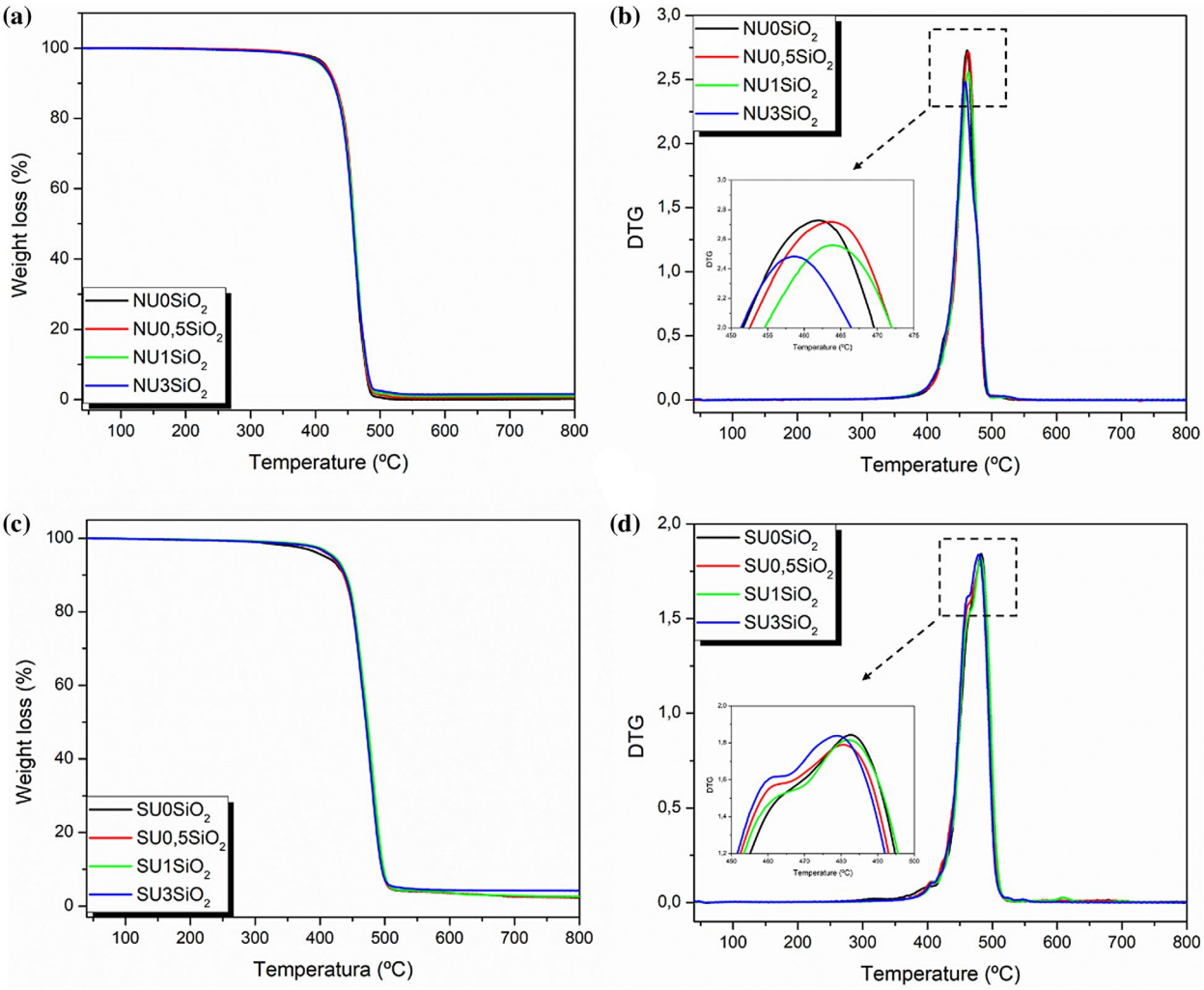

Figure 5. TGA and DTG thermograms for (a-b) EMAA copolymer and its SiO_2-reinforced nanocomposites and (c-d) EMAA-Na ionomer and its SiO_2-reinforced nanocomposites.

Figure 7 presents an example of the stress-strain curves obtained for all the EMAA-based materials. It is possible to easily notice that the neutralization of the EMAA copolymer provokes an increase of the mechanical properties. In fact EMAA-Na ionomer-based materials showed higher elastic modulus and higher maximum stress values compared to EMAA copolymer-based materials. On the other hand, elongation at break decreased for EMAA-Na ionomer due to the Na neutralization of methacrylic acid groups. The mechanical properties of all the processed materials are summarized in Table 2.

The presence of the SiO_2 nanoparticles in the EMAA-based materials, affect the mechanical properties increasing the elastic modulus, which reach maximum values when the materials were filled with 1 wt.% of SiO_2 nanoparticle. In particular, in the case of $NU1SiO_2$ the elastic modulus was almost three times that of its neat counterpart probably due to the good interaction between the acid groups in the polymeric chain and the silica nanoparticles. For $SU1SiO_2$ was not so evident probably because the mechanical properties are controlled more from the ionomeric cluster formed in the structure. Otherwise, when 3 wt.% of SiO_2 nanoparticles were used, the elastic modulus remained constant for $NU3SiO_2$ although it significantly decreased in the case of $SU3SiO_2$. However, maximum stress values were not affected by the presence of SiO_2 nanoparticles, while elongation at break slightly decreased for both series of EMAA- and EMAA-Na-based materials.

Based on the microstructure of EMAA copolymer and EMAA-Na ionomer resin, as well as their thermal and mechanical properties, the parameters for the thermo-mechanical cycles were established in order to study their shape-memory response. As discussed before, EMAA copolymer and ionomer resin are complex systems, composed by PE crystals, amorphous polymer chains and ionic aggregates, in the case of the ionomer resin. Figure 8 shows a schematic representation of the complex microstructure of both EMAA-based materials. In the non-neutralized copolymers, the amorphous phase is composed primarily of polyethylene with some isolated or hydrogen bonded methacrylic acid groups and a crystalline polyethylene phase (Figure 8(a)). For the EMAA-Na ionomer resin the amorphous phase contain isolated or hydrogen bonded methacrylic acid groups, contact ion pairs and multiplets of ion pairs as

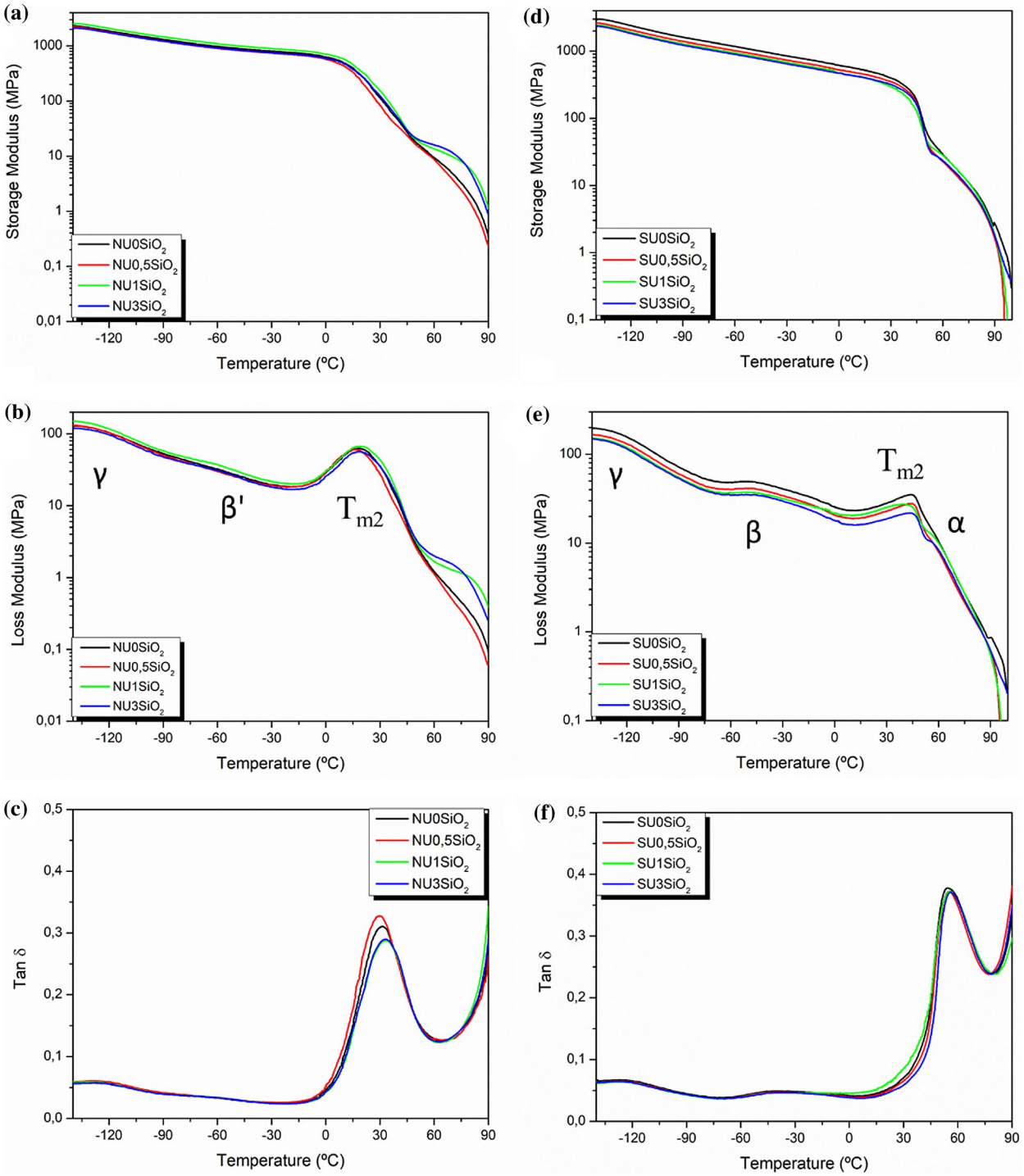

Figure 6. Dynamic mechanical properties: storage modulus (E′), loss modulus (E″) and damping factor (tanδ) as a function of temperature of a-b-c) EMAA copolymer and its SiO_2-reinforced nanocomposites and d-e-f) EMAA-Na ionomer and its SiO_2-reinforced nanocomposites.

well as ionic nanophase (the ionic clusters) that contains most of the ion pairs (Figure 8(b)) [21].

In our previous work, the thermally activated shape memory effect of neat ethylene-vinyl acetate copolymer and its blends with thermoplastic starch has been studied by using the stretch-induced crystallization mechanism to induce the temporary shape [16]. Indeed, it was demonstrated that a new poorly organized crystalline structure (A phase), induced by stretching the samples until 250% of elongation at 40 °C, was used as switching phase while the higher organized structure closer to that of pure polyethylene (B phase) was used as permanent phase. Therefore, the T_m of A crystal phase was considered the switching temperature (T_{sw}) of our systems [16]. Thus, based on our past results and on other works reporting the shape memory behavior of systems with two distinct melting points [14,58], in this work, we study the thermally activated shape memory response of EMAA copolymer-based materials considering that the smaller PE secondary crystals act as switching network,

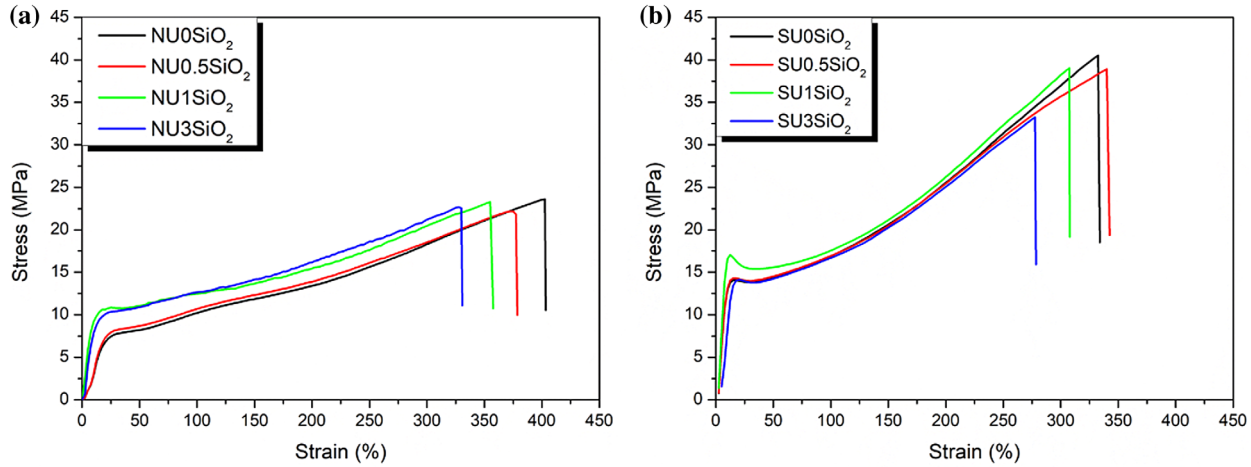

Figure 7. Stress–strain curves for (a) EMAA copolymer and its SiO_2-reinforced nanocomposites and (b) EMAA-Na ionomer and its SiO_2-reinforced nanocomposites.

Table 2. Mechanical properties of the processed materials.

Sample	Elastic Modulus (MPa)	Maximum stress (MPa)	Elongation at break (%)
$NU0SiO_2$	52 ± 3	23 ± 1	408 ± 11
$NU0.5SiO_2$	58 ± 6	22 ± 1	370 ± 9
$NU1SiO_2$	138 ± 8	24 ± 1	357 ± 23
$NU3SiO_2$	134 ± 6	23 ± 1	332 ± 9
$SU0SiO_2$	198 ± 8	41 ± 3	338 ± 28
$SU0.5SiO_2$	196 ± 10	41 ± 3	342 ± 20
$SU1SiO_2$	252 ± 6	39 ± 2	311 ± 17
$SU3SiO_2$	149 ± 25	34 ± 4	283 ± 25

being able to fix the temporary shape and the PE primary crystals together with the amorphous phase act as permanent network, memorizing the original shape. Therefore, a temperature above the T_m of the PE secondary crystals was taken as T_{sw}.

On the other hand, for EMAA-Na ionomer-based materials we considered that PE crystals (both secondary and primary crystals) act as the switching network while the permanent network is ensured by the ionic interaction and the ionic clusters. Furthermore, systems characterized by a broad melting transition, due to a wide distribution of crystallite sizes, may also be used to produce multiple thermally activated shape memory material, as previously reported in literature [21,59]. Indeed, in ionomers, the crystalline phase can provide a physical switching network to fix one or multiple temporary shapes and the ionic clusters may be sufficiently strong to provide a permanent network and recover the original shape.

The dual-shape memory behavior of all the samples, based on EMAA copolymer as well as on EMAA-Na ionomer, was studied by DMTA for quantification performing 4 consecutive cycles. The dual-shape thermo-mechanical cycles were performed at 50% of elongation. The programming step was designed with a uniaxial stretching at 60 °C as T_{sw}, followed by a fast quenching of the stretched state at 0 °C (T_{fix}). The stretched state was maintained after quenching and subsequent removal of the stress at the same temperature. Then the recovery was activated at the specific T_{sw}. Figure 9 shows the evolution of strain, stress, and temperature during the dual-shape memory programming step and the consequent free-strain recovery for the EMAA copolymer and its SiO_2-reinforced nanocomposites.

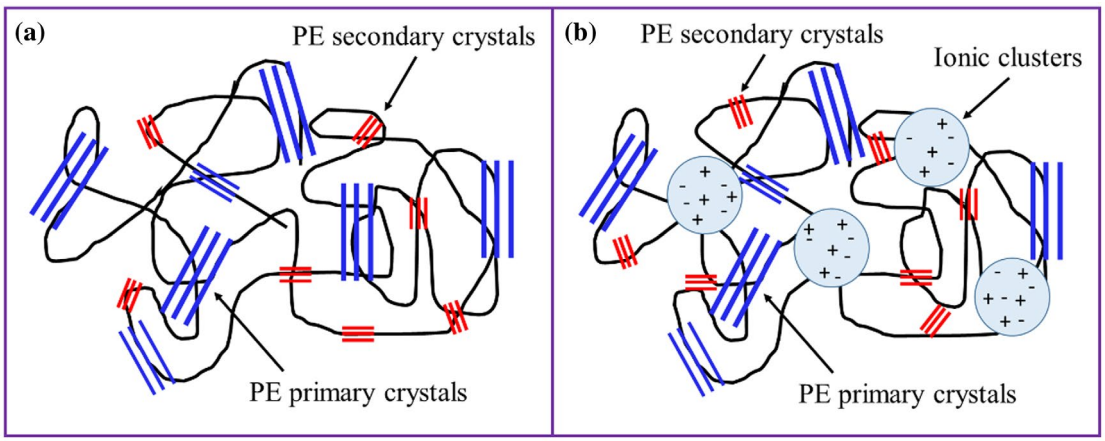

Figure 8. Schematic representation of the microstructure of (a) EMAA copolymer and (b) EMAA-Na ionomer.

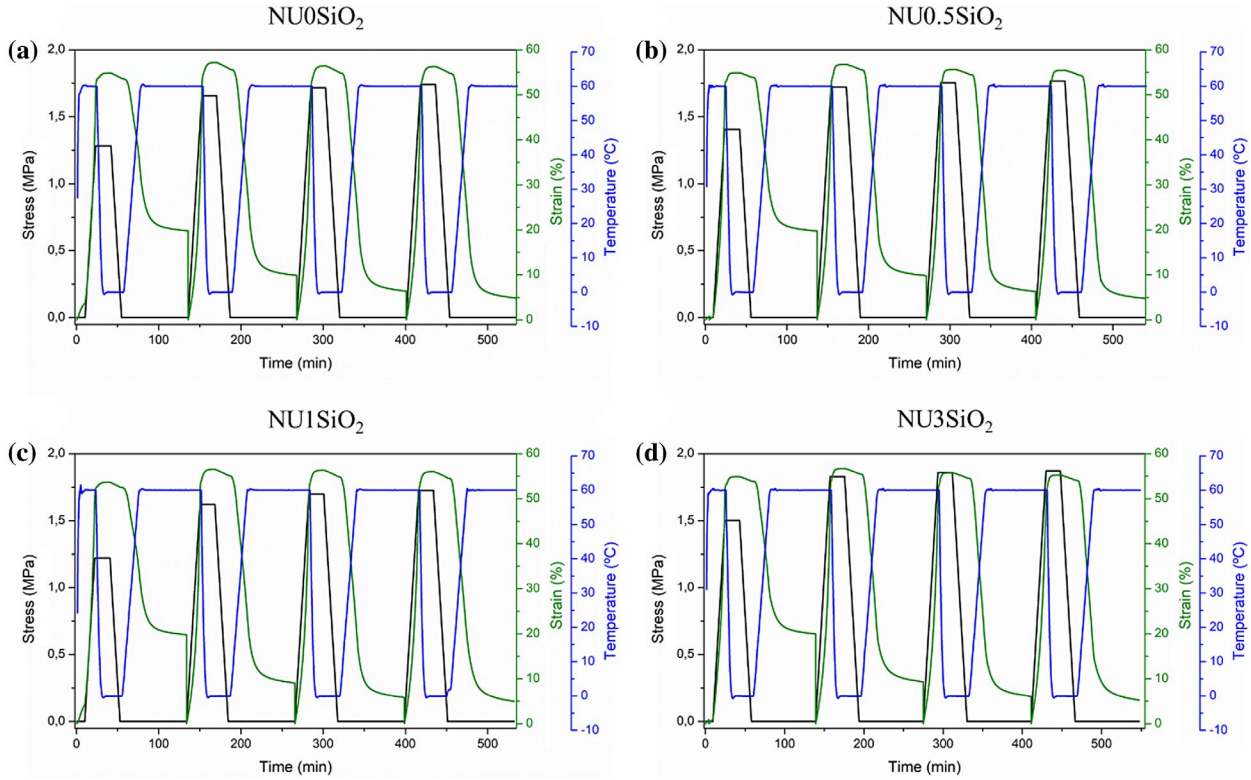

Figure 9. Dual-shape thermo-mechanical cycles of EMAA copolymer: (a) NU0SiO$_2$, (b) NU0.5SiO$_2$, (c) NU1SiO$_2$, and (d) NU3SiO$_2$.

It is worth to notice that all the samples showed an increase of the applied stress between cycle 0 and cycle 1, remaining then in a constant value. The presence of the SiO$_2$ did not affect the applied stress value comparing the different nanocomposites, although a slightly increase of the applied stress was observed only for NU3SiO$_2$. On the other hand, we can claim that any failure at the interface between polymer/inorganic nanoparticles occurred, since a decrease of the applied stress was not observed but it remained constant during the consecutive cycles. All the samples shown good ability to fix the deformed shape at the selected T_{fix} while the recovery process begun before reaching the selected T_{sw}, as was expected observing the DSC thermogram reported in Figure 4(c), where the onset of the melting peak is at around 30 °C. At the selected T_{sw}, the sample needed 15 min to recover almost the maximum, reaching a plateau. In Table 3, the results of the thermo-mechanical cycles in terms of R_r and R_f are summarized for EMAA copolymer and its SiO$_2$-reinforced nanocomposites.

As can be noted, NU0SiO$_2$ and its nanocomposites have shown excellent shape memory properties reaching values higher than 83% and 97% for R_r and R_f, respectively. Increasing the SiO$_2$ amount in the nanocomposites, a slight increase in the R_r was observed, reaching maximum values for NU1SiO$_2$.

Figure 10 shows the evolution of strain, stress, and temperature during the dual-shape memory programming step and the consequent free-strain recovery for the EMAA-Na ionomer resin and its SiO$_2$-reinforced nanocomposites.

Table 3. R_r and R_f values obtained by dual-shape thermo-mechanical cycles for EMAA copolymer and its SiO$_2$-reinforced nanocomposites.

Sample	R_r (%)			R_f (%)		
Cycles	1	2	3	1	2	3
NU0SiO$_2$	83	89	91	98	97	97
NU0.5SiO$_2$	84	90	91	98	98	98
NU1SiO$_2$	85	90	91	98	98	98
NU3SiO$_2$	83	88	89	98	98	98

Compared with EMAA copolymer-based materials, EMAA-Na ionomer showed higher values of applied stress, due to the methacrylic acid group neutralization, as previously observed for the mechanical properties. Moreover, the applied stress values increase gradually increasing the number of cycles but was not affected by the presence of SiO$_2$ in the nanocomposites. As for EMAA copolymer-based materials, in Figure 9 it is shown that the recovery process for EMAA-Na ionomer-based materials begun before reaching the T_{sw} of 60 °C. In particular, in this case, the recovery process starts 10 °C higher compared with EMAA copolymer-based materials, thus confirming the DSC and DMTA results. At the selected T_{sw}, the sample needed 20 min to recover almost the maximum, reaching a plateau. Compared with EMAA copolymer, they takes more time to recover the original shape probably due to the high interactions between the polymeric chains and the ionomeric clusters that lead to a decrease of the chain mobility. In Table 4, the results of thermo-mechanical cycles in terms of R_r and R_f are summarized for

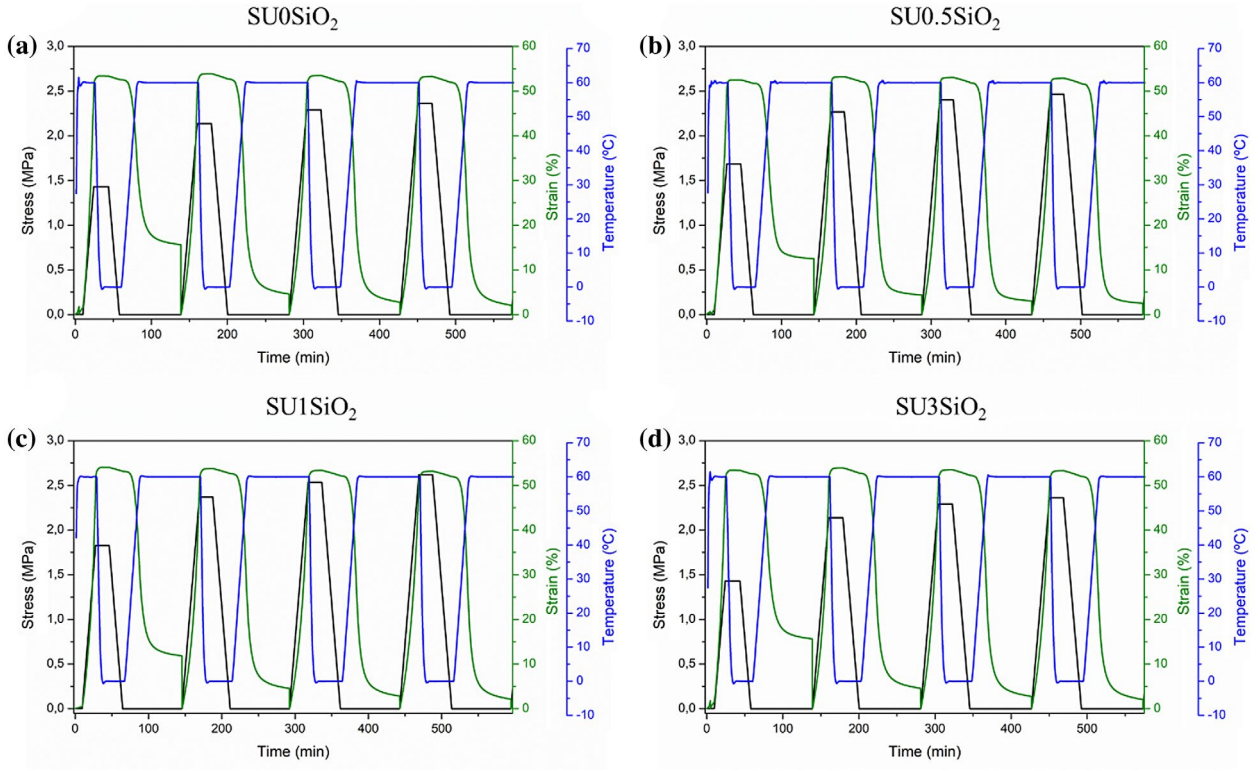

Figure 10. Dual-shape thermo-mechanical cycles of EMAA-Na ionomer resin (a) $SU0SiO_2$, (b) $SU0.5SiO_2$, (c) $SU1SiO_2$, and (d) $SU3SiO_2$.

Table 4. R_r and R_f values obtained by dual-shape thermo-mechanical cycles for EMAA-Na ionomer and its SiO_2-reinforced nanocomposites.

Sample	R_r (%)			R_f (%)		
Cycles	1	2	3	1	2	3
$SU0SiO_2$	91	95	96	98	98	98
$SU0.5SiO_2$	92	94	96	98	98	98
$SU1SiO_2$	92	95	96	98	98	98
$SU3SiO_2$	88	91	95	98	98	97

EMAA ionomer and its nanocomposites. As can be seen, $SU0SiO_2$ and its nanocomposites have shown excellent shape memory properties reaching maximum values of about 96 and 98% for R_r and R_f, respectively.

An ideal system presents both R values of 100%, which mean that it is able to totally recover its original shape as well as to completely fix its temporary shape. Therefore, values of R_r below 100% indicate defects in the ionic network used as the permanent network for EMAA. While R_f values lower than 100% probably are due to the presence of a broad crystalline phase in the structure, as previously obtained. Moreover, the difference from the ideal system may be due to creep recovery of the network chains connected to the ionic domains, which can occur as a consequence of the physical nature of these crosslinks, as was already reported in literature [21].

It is well known that the addition of nanoparticles to the polymer matrix can change their properties in term of crystallinity, mechanical response and also compatibility between different phases, affecting the shape memory response of the nanocomposites. Therefore, it is not trivial that when the polymeric matrix presents shape memory effect, the same effect will be encountered in its nanocomposites. An example is reported by Navarro-Baena et al. where they reported that the transition temperature for the neat polymeric matrix is slightly different that the one used for the bionanocomposites as a consequence of the addition of nanofillers [17].

However, in our case it is quite difficult to get better result on the shape memory response respect to the excellent one of the polymeric matrix (R_r = 91%, R_f = 97% for Nucrel and R_r = 96%, R_f = 98% for Surlyn). However, the addition of nanoparticles does not worsen this response and also increase the mechanical response of the nanocomposites respect to the neat matrix at the same transition temperature, maintaining the excellent shape memory response (R_r = 91%, R_f = 98% for $NU1SiO_2$ and R_r = 96%, R_f = 98% for $SU1SiO_2$ taken as the best nanocomposites obtained). In particular, in the case of NU1SiO2 the elastic modulus was almost three times that of its neat counterpart probably due to the good interaction between the acid groups in the polymeric chain and the silica nanoparticles. Therefore, nowadays, to study the effect of the incorporation of nanofillers in shape memory systems is a very important challenge to be deeply explored. Based on our knowledge this is the first time that the shape memory response of Surlyn® and Nucrel® reinforced with silica nanoparticles has been studied.

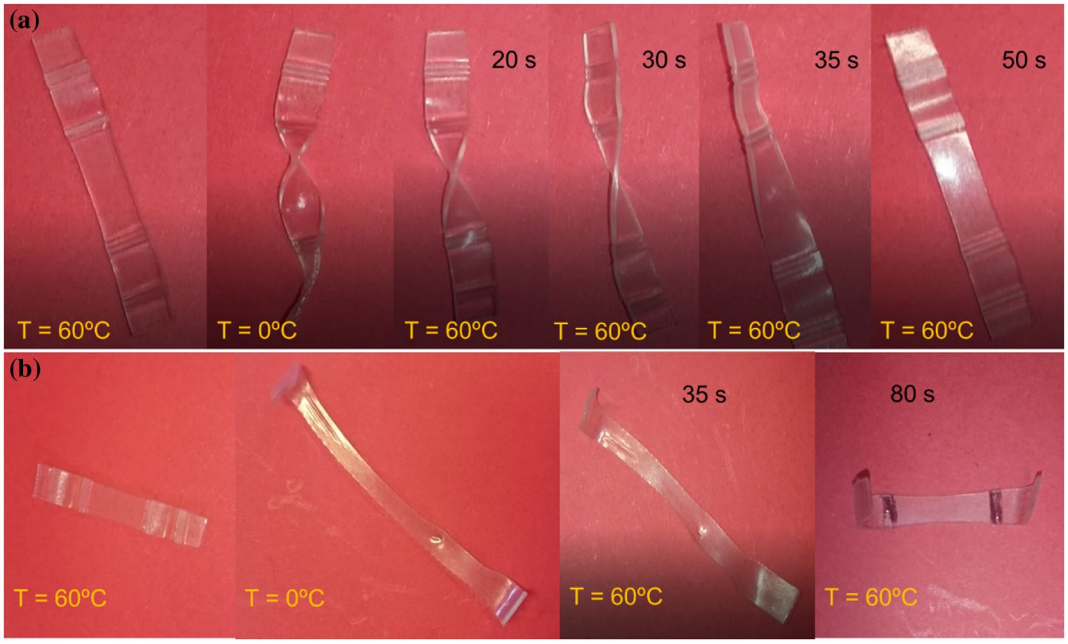

Figure 11. Example of shape memory response of Surlyn® direct triggered at 60 °C to activate the recovery of the original shape, starting from a twisted temporary shape (a) as well as from a stretched temporary shape (b).

However, Dolog and Weiss investigated a zinc neutralized ethylene-co-methacrylic acid ionomer, commercially available as Surlyn®9520 [20,21]. They reported that the ionic aggregates are able to serve as the physically crosslinked permanent network, while the crystallization of the polyethylene segments forms the second temporary network resulting in shape memory behavior. Very good shape memory behavior was observed by dynamic mechanical testing with a strain fixity ratio of 99% and a strain recovery ratio of 72%, in the first cycle, which improved to 99 and 88%, respectively, in the second cycle at 105 °C. They attribute the lower recovery to the stress relaxation of the ionic domains [20,21]. Moreover, they studied the shape memory response at different temperature, from 60 to 105 °C and at 60 °C, they obtain a strain fixity ratio of 78% and a strain recovery ratio of 88%, a little bit smaller than the excellent values obtained by us. They also studied shape memory behavior of compounds formed from a commercial poly(ethylene-co-methacrylic acid) ionomer and zinc stearate (ZnSt) [25]. They found that a compound containing 50 wt.% ZnSt where nanophase-separated ionic aggregates acted as a permanent network and a phase-separated ZnSt crystalline phase was a reversible network showed shape memory behavior repeatable over five consecutive shape memory cycles with shape fixity and shape recovery values of ~92% and ~97%, respectively. Zhao et al. [26] also studied the shape memory effect on Zinc-Neutralized Poly(ethylene-co-methacrylic acid) and they reported values of $F = 80.9\%$ and $R = 82.5\%$ at 70 °C during the first cycle, and values of shape fixity and shape recovery of about 75 and 99%, respectively, in the further cycles. Lu and Li, reported a study on one-way multi-shape memory effect and tunable two-way shape memory effect of ionomer based on poly(ethylene-co-methacrylic acid) [27]. They proposed the crystallization-melting driven process as mechanism for the tunable two-way shape memory effect. They also reported that a class of thermally reversible polymers may find applications in real life such as actuators, fixator, sealant, artificial muscles, etc.

However, they are able to respond very quickly if they are directly triggered at the transition temperature. In fact, when the samples are heated and deformed in their temporary shape, and they are directly triggered in an oven at 60 °C, they are able to recover its original shape in few minutes. To confirm this fact, two examples are reported in Figure 11, stretching as well as twisting the sample where the quickly recuperation of the original shape can be confirmed. In fact, in less than 1 min the sample is able to completely recover its original shape when it is twisted, and it need 80 s to recover its original shape when it is stretched.

As was mentioned above, for the EMAA-Na ionomer-based materials it is possible to perform the thermally activated triple-shape memory cycles, thanks to the broad melting transition of PE crystals, that permit to program different temporary shapes, and the ionic permanent network which is stable at temperatures above the highest melting temperature of the system. In Figure 12, an example of triple shape diagram is reported as evolution of stress, strain and temperature in function of time emphasizing the different stages and the different changes of the shape. As was reported in Figure 1(b), the entire cycle is composed by the programming and the recovery stage. In the programming stage, 2 different temporary shapes, i.e. shapes 2 and 3, were programmed at 80 and 60 °C

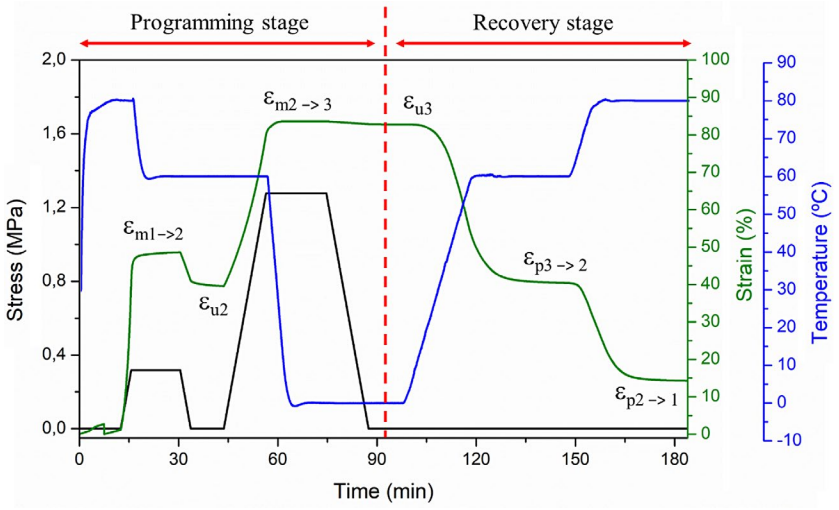

Figure 12. Schematic representation of a triple-shape thermo-mechanical cycle.

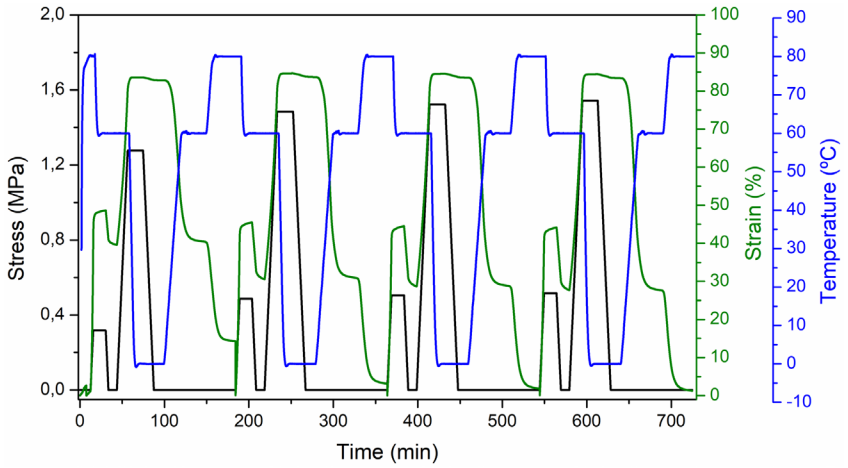

Figure 13. Triple-shape thermo-mechanical cycles of SU1SiO$_2$.

with applied stresses of about 0.5 and 1.5 MPa, respectively. The sample was first heated at the higher T_{sw}, called T_{sw1} (80 °C) and stretched until 40% of strain (ε_{m1-2}). Then, the sample was cooled at 60 °C in order to fix the first temporary shape and consequently the applied stress was released (ε_{u2}). At the same temperature (60 °C) the sample was stretched until 80% of strain (ε_{m2-3}) and cooled down at the T_{fix} (0 °C) to fix the second temporary shape and then the applied stress was released (ε_{u3}). At this time, first and second temporary shapes are both programmed and the recovery stage can be started heating before at the lowest T_{sw} (60 °C) and finally at the highest T_{sw} (80 °C) in order to recover the second and the original shapes, respectively.

The triple-shape memory behavior of SU1SiO$_2$, as the best sample between EMAA ionomer-based materials, was studied by DMTA for quantification performing 4 consecutive cycles. Figure 13 shows the evolution of strain, stress, and temperature during the triple-shape memory programming step and the consequent free-strain recovery for SU1SiO$_2$. From the evolution of the strain during the overall thermo-mechanical cycle, several quantitative parameters are defined to evaluate triple-shape memory performances, similar to dual-shape memory experiments: the strain fixity ratio of the shapes 2 and 3 and the strain recovery ratio of the shapes 1 and 2. At this regard, Equations (2) and (3) developed for dual-shape memory experiments could be generalized by Equations (4) and (5) for multiple-shape memory experiments.

$$R_{r\,Sj\to i} = \frac{\left(\varepsilon_{uj} - \varepsilon_{pi}\right)}{\left(\varepsilon_{uj} - \varepsilon_{ui}\right)} \times 100\% \tag{4}$$

$$R_{f\,Si\to j} = \frac{\left(\varepsilon_{uj} - \varepsilon_{ui}\right)}{\left(\varepsilon_{mj} - \varepsilon_{ui}\right)} \times 100\% \tag{5}$$

Table 5. R_r and R_f values obtained by triple-shape thermo-mechanical cycles for $SU1SiO_2$.

Sample	$R_{r\,S2\to1}$ (%)			$R_{r\,S3\to2}$ (%)			$R_{fS1\to2}$ (%)			$R_{fS2\to3}$ (%)		
Cycles	1	2	3	1	2	3	1	2	3	1	2	3
$SU1SiO_2$	90	94	95	100	100	100	68	65	63	99	99	99

where, i and j represent the different shapes while ε_m, ε_u, and ε_p denote the deformed, fixed, and recovered strain, respectively.

The shape fixity and recovery values for the triple shape memory cycles shown in Figure 13 are listed in Table 5.

Figure 13 shows that a strain (ε_{m1-2}) of 50% was achieved after the first uniaxial stretching at 80 °C and cooling to 60 °C. The strain clearly decreased after unloading at 60 °C and reached a final value of 40% (ε_{u2}). A strain (ε_{m2-3}) of 84% is reached after the second stretching at 60 °C, and a final strain (ε_{u3}) of 83% could be fixed at 0 °C, indicating full crystallization of the PE crystals. Concerning the recovery of shape 2 at 60 °C, a progressive strain decrease was observed from 83 to 41%, and the strain recovery ratio related to shape 2 ($R_{r\,S3\to2}$) is subsequently evaluated to 98%. In this respect, a good control over shape 2 could be obtained for the $SU1SiO_2$ according with the $R_{r\,S3\to2}$ values obtained during the consecutive cycles ($R_{r\,S3\to2}$ 100%) and the previous dual-shape memory experiments. Then, shape 1 is subsequently recovered at high temperature (80 °C) with a residual strain close to 15% ($R_{r\,S2\to1}$ 64%), indicating that the fixed shape 2 partially relaxed because the fraction of material recrystallized at the first cooling was not enough to well fix the shape 2. Otherwise, the $R_{r\,S2\to1}$ during the consecutive cycles performed, were pretty good reaching values higher than 90%. If the fraction of material recrystallized is not enough, the sample has insufficient strength to oppose the stress developed during the programming of the shape 2. This fact lead to strain fixity ratios related to the shape 2 lower than that related to the shape 3. Indeed, the fraction of polymer that recrystallized to form the temporary network was probably lower at 60 °C than at 0 °C. On the other hand, the strain fixity ratios related to the shape 3, reached values of 99% for all the cycles performed indicating that the fraction of recrystallized PE crystals was always enough to well fix the second temporary shape.

Conclusions

EMAA copolymers and their ionomers nanocomposites reinforced with SiO_2 nanoparticles were melt-processed in this work. Morphological, thermal and mechanical properties were studied, as well as the dynamic thermo-mechanical and shape memory behavior. A good dispersion of SiO_2 nanoparticles was observed for all the EMAA-based nanocomposites although an improvement of the dispersion was noticed in the case of EMAA-Na nanocomposites. EMAA-based materials showed a complex thermal and thermo-mechanical behavior due to their complex morphology composed of polyethylene (PE) crystals, amorphous polymer chains, and ionic aggregates, in the case of ionomers. In this work, we followed the model that ascribes the lower temperature endothermic peak on DSC thermograms to the PE secondary crystals. The presence of the SiO_2 nanoparticles did not affect the thermal properties of all the processed materials. Otherwise, the presence of the SiO_2 nanoparticles in the EMAA-based materials, did affect the mechanical properties increasing the elastic modulus, which reach the maximum values when the materials were filled with 1 wt.% of SiO_2 nanoparticle. The thermally activated shape memory response of EMAA copolymer-based materials was studied considering that the smaller PE secondary crystals act as switching network, being able to fix the temporary shape and the PE primary crystals together with the amorphous phase act as permanent network, memorizing the original shape. Therefore, a temperature above the T_m of the PE secondary crystals was taken as T_{sw}. On the other hand, for EMAA-Na ionomer-based materials we considered that PE crystals (both secondary and primary crystals) act as the switching network while the permanent network is ensured by the ionic interaction and the ionic clusters. As it is possible to note, EMAA copolymer and its nanocomposites showed excellent shape memory properties reaching values higher than 83 and 97% for R_r and R_f, respectively. Increasing the SiO_2 amount in the nanocomposites, a slight increase in the R_r that reach maximum values for $NU1SiO_2$ was observed. Moreover, EMAA-Na ionomer resin and its nanocomposites showed excellent shape memory properties reaching maximum values of about 96 and 98% for R_r and R_f, respectively. Thermally activated triple-shape memory cycles were performed for $SU1SiO_2$ as the best EMAA-Na-based nanocomposite, using the broad melting transition of PE crystals to program different temporary shapes and considering that the ionic permanent network was still stable at temperature above the highest meting temperature of the system showing excellence response in term of R_r and R_f in both temporary forms.

Acknowledgments

Authors thank the Spanish Ministry of Economy, Industry and Competitiveness (MINEICO) (MAT2017-88123-P, POLYMAGIC: PCIN-2017-036) and the Regional Government of Madrid (MULTIMAT CHALLENGE: S2013/MIT-2862). L.P. acknowledges the 'Ramon y Cajal' (RYC-2014-15595) contract from MINEICO.

Disclosure statement

No potential conflict of interest was reported by the authors.

Notes on contributors

Valentina Sessini is a postdoc researcher at the Laboratory of Polymeric and composites materials of the University of Mons (Belgium). She has published mainly on biocompatible and biodegradable thermally- and humidity-activated shape memory polymers and nanocomposites.

David Brox is graduated student in the department of Applied Mathematics, Science and Engineering of Materials and Electronic Technology at the Rey Juan Carlos University. He has worked on thermally-activated shape memory nanocomposites based on ethylene copolymers and ionomers.

Antonio Julio López is associate professor of materials science and metallurgy engineering at the Applied Mathematics, Materials Science and Engineering and Electronic Technologies, Rey Juan Carlos University. He has published more than 35 papers in the surface engineering, tribology, corrosion and polymer fields. He is also the author of three book chapters.

Alejandro Ureña is full professor of materials science and metallurgy engineering at the Applied Mathematics, Materials Science and Engineering and Electronic Technologies, Rey Juan Carlos University. He has published more than 100 papers in the welding, composite material and polymer fields. He is an active member and former president of the Spanish Composite Material Association (MATCOMP).

Laura Peponi is a "Ramon y Cajal" researcher at the Institute of Polymer Science and Technology ICTP, of CSIC, in Madrid, Spain. She has published more than 60 scientific papers on multifunctional polymeric nanocomposites focusing her attention in the last years on multi shape memory polymers

References

1 Arrieta MP, Sessini V, Peponi L. Biodegradable poly(ester-urethane) incorporated with catechin with shape memory and antioxidant activity for food packaging. Eur Polym J. 2017;94:111–124.
2 Peponi L, Navarro-Baena I, Sonseca A, et al. Synthesis and characterization of PCL-PLLA polyurethane with shape memory behavior. Eur Polym J. 2013;49(4):893–903.
3 Rousseau IA. Challenges of shape memory polymers: A review of the progress toward overcoming SMP's limitations. Polym Eng Sci. 2008;48(11):2075–2089.
4 Sessini V, Arrieta MP, Fernández-Torres A, et al. Humidity-activated shape memory effect on plasticized starch-based biomaterials. Carbohyd Polym. 2018;179:93–99.
5 Wang CC, Huang WM, Ding Z, et al. Cooling-/water-responsive shape memory hybrids. Compos Sci Technol. 2012;72(10):1178–1182.
6 Lee YM, Kim SH, Cho CS. Synthesis and swelling characteristics of pH and thermoresponsive interpenetrating polymer network hydrogel composed of poly (vinyl alcohol) and poly (acrylic acid). J Appl Polym Sci. 1996;62(2):301–311.
7 Lendlein A, Jiang H, Jünger O, et al. Light-induced shape-memory polymers. Nature. 2005;434(7035):879–882.
8 Liu Y, Lv H, Lan X, et al. Review of electro-active shape-memory polymer composite. Compos Sci Technol. 2009;69(13):2064–2068.
9 Peponi L, Navarro-Baena I, Kenny J. Shape memory polymers: properties, synthesis and applications. In: Aguilar MR, De Armas JSR, editor. Smart polymers and their applications. Oxford: Elsevier; 2014. p. 204–236.
10 Sessini V, Raquez JM, Lourdin D, et al. Humidity-activated shape memory effects on thermoplastic starch/EVA blends and their compatibilized Nanocomposites. Macromol Chem Phys. 2017;218(24):1700388.
11 Meng Q, Hu J. A review of shape memory polymer composites and blends. Compos Part A-Appl S. 2009;40(11):1661–1672.
12 Peponi L, Arrieta MP, Mujica-Garcia A, et al. Smart polymers. In: Jasso-Gastinel CF, Kenny JM, editors, Modification of Polymer Properties. Chadds Ford (PA); 2016. p. 131–154.
13 Behl M, Lendlein A. Triple-shape polymers. J Mater Chem. 2010;20(17):3335–3345.
14 Bellin I, Kelch S, Lendlein A. Dual-shape properties of triple-shape polymer networks with crystallizable network segments and grafted side chains. J Mater Chem. 2007;17(28):2885–2891.
15 Bellin I, Kelch S, Langer R, et al. Polymeric triple-shape materials. Proc Natl Acad Sci USA. 2006;103(48):18043–18047.
16 Sessini V, Raquez J-M, Lo Re G, et al. Multiresponsive Shape Memory Blends and Nanocomposites Based on Starch. ACS Appl Mater Int. 2016;8(30):19197–19201.
17 Navarro-Baena I, Kenny J, Peponi L. Thermally-activated shape memory behaviour of bionanocomposites reinforced with cellulose nanocrystals. Cellulose. 2014;21(6):4231–4246.
18 Lendlein A, Kelch S. Shape-memory polymers. Angew Chem Int Ed. 2002;41(12):2034–2057.
19 Zhang L, Brostowitz NR, Cavicchi KA, et al. Perspective: ionomer research and applications. Macromol React Eng. 2014;8(2):81–99.
20 Cavicchi KA, Pantoja M, Cakmak M. Shape memory ionomers. J Polym Sci Pol Phys. 2016;54(14):1389–1396.
21 Dolog R, Weiss R. Shape memory behavior of a polyethylene-based carboxylate ionomer. Macromolecules. 2013;46(19):7845–7852.
22 Varley RJ, Shen S, van der Zwaag S. The effect of cluster plasticisation on the self healing behaviour of ionomers. Polymer. 2010;51(3):679–686.
23 Varley RJ, van der Zwaag S. Towards an understanding of thermally activated self-healing of an ionomer system during ballistic penetration. Acta Mater. 2008;56(19):5737–5750.
24 Francesconi A, Giacomuzzo C, Grande A, et al. Comparison of self-healing ionomer to aluminium-alloy bumpers for protecting spacecraft equipment from space debris impacts. Adv Space Res. 2013;51(5):930–940.
25 Dolog R, Weiss R. Properties and shape-memory behavior of compounds of a poly (ethylene-co-methacrylic acid) ionomer and zinc stearate. Polymer. 2017;128:128–134.
26 Zhao Z, Peng F, Cavicchi KA, et al. Three-Dimensional Printed Shape Memory Objects Based on an Olefin Ionomer of Zinc-Neutralized Poly (ethylene-co-methacrylic acid). ACS Appl Mater. Inter. 2017;9(32):27239–27249.
27 Lu L, Li G. One-way multishape-memory effect and tunable two-way shape memory effect of ionomer poly

(ethylene-co-methacrylic acid). ACS Appl Mater Int. 2016;8(23):14812–14823.
28 Pilate F, Toncheva A, Dubois P, et al. Shape-memory polymers for multiple applications in the materials world. Eur Polym J. 2016;80:268–294.
29 Peponi L, Puglia D, Torre L, et al. Processing of nanostructured polymers and advanced polymeric based nanocomposites. Mater Sci Eng R Rep. 2014;85(1):1–46.
30 Schadler L, Giannaris SA, Ajayan P. Load transfer in carbon nanotube epoxy composites. Appl Phys Lett. 1998;73(26):3842–3844.
31 Yao Z, Kane CL, Dekker C. High-field electrical transport in single-wall carbon nanotubes. Phys Rev Lett. 2000;84(13):2941.
32 Lu H, Liu Y, Gou J, et al. Electrical properties and shape-memory behavior of self-assembled carbon nanofiber nanopaper incorporated with shape-memory polymer. Smart Mater Struct. 2010;19(7):075021.
33 Yu K, Liu Y, Leng J. Shape memory polymer/CNT composites and their microwave induced shape memory behaviors. RSC Adv. 2014;4(6):2961–2968.
34 Wang L, Wang W, Di S, et al. Silver-coordination polymer network combining antibacterial action and shape memory capabilities. RSC Adv. 2014;4(61):32276–32282.
35 Zhang H, Zhao Y. Polymers with dual light-triggered functions of shape memory and healing using gold nanoparticles. ACS Appl Mater Int. 2013;5(24):13069–13075.
36 Mohr R, Kratz K, Weigel T, et al. Initiation of shape-memory effect by inductive heating of magnetic nanoparticles in thermoplastic polymers. Proc Natl Acad Sci USA. 2006;103(10):3540–3545.
37 Zheng X, Zhou S, Xiao Y, et al. Shape memory effect of poly (d, l-lactide)/Fe3O4 nanocomposites by inductive heating of magnetite particles. Colloid Surface B. 2009;71(1):67–72.
38 Odent Jrm, Raquez J-M, Samuel CD, et al. Shape-Memory Behavior of Polylactide/Silica Ionic Hybrids. Macromolecules. 2017;50(7):2896–2905.
39 Kwon D-J, Shin P-S, Kim J-H, et al. Interfacial properties and thermal aging of glass fiber/epoxy composites reinforced with SiC and SiO2 nanoparticles. Compos Part B-Eng. 2017;130:46–53.
40 Jia X, Li G, Liu B, et al. Multiscale reinforcement and interfacial strengthening on epoxy-based composites by silica nanoparticle-multiwalled carbon nanotube complex. Compos Part A-Appl S. 2013;48:101–109.
41 Odent J, Raquez J-M, Thomassin J-M, et al. Mechanistic insights on nanosilica self-networking inducing ultra-toughness of rubber-modified polylactide-based materials. Nanocomposites. 2015;1(3):113–125.
42 Salgado C, Arrieta MP, Peponi L, et al. Silica-nanocomposites of photo-crosslinkable poly (urethane) s based on poly (ε-caprolactone) and coumarin. Eur Polym J. 2017;93:21–32.
43 Wunderlich B. Molecular physics, Volume 3: crystal melting. New York (NY): Academic Press; 1980.
44 Longworth R, Vaughan DJ. Physical structure of ionomers. Nature. 1968;218:85–87.
45 Loo Y-L, Wakabayashi K, Huang YE, et al. Thin crystal melting produces the low-temperature endotherm in ethylene/methacrylic acid ionomers. Polymer. 2005;46(14):5118–5124.
46 Marx CL, Cooper SL. The crystallinity of ionomers. J Macromol Sci B. 1974;9(1):19–33.
47 Kuwabara K, Horii F. Solid-state NMR analyses of the crystalline–noncrystalline structure and its thermal changes for ethylene ionomers. J Polym Sci Pol Phys. 2002;40(11):1142–1153.
48 Tsujita Y, Shibayama K, Takizawa A, et al. Thermal properties of ethylene ionomers. J Appl Polym Sci. 1987;33(4):1307–1314.
49 Hirasawa E, Yamamoto Y, Tadano K, et al. Formation of ionic crystallites and its effect on the modulus of ethylene ionomers. Macromolecules. 1989;22(6):2776–2780.
50 Ray A. Effects of chemical constituents on crystalline properties of ethylene ionomers. J Therm Anal Calorim. 1996;46(6):1527–1539.
51 Tachino H, Hara H, Hirasawa E, et al. Dynamic mechanical relaxations of ethylene ionomers. Macromolecules. 1993;26(4):752–757.
52 Tadano K, Hirasawa E, Yamamoto H, et al. Order-disorder transition of ionic clusters in ionomers. Macromolecules. 1989;22(1):226–233.
53 Dong J, Weiss RA. Shape memory behavior of zinc oleate-filled elastomeric ionomers. Macromolecules. 2011;44(22):8871–8879.
54 Siuzdak DA, Start PR, Mauritz KA. Surlyn®/silicate hybrid materials. I. Polymer in situ sol–gel process and structure characterization. J Appl Polym Sci. 2000;77(13):2832–2844.
55 Kutsumizu S, Nagao N, Tadano K, et al. Effects of water sorption on the structure and properties of ethylene ionomers. Macromolecules. 1992;25(25):6829–6835.
56 Eisenberg A, Navratil M. Ion clustering and viscoelastic relaxation in styrene-based ionomers. IV. X-ray and dynamic mechanical studies. Macromolecules. 1974;7(1):90–94.
57 Wakabayashi K, Register RA. Morphological origin of the multistep relaxation behavior in semicrystalline ethylene/methacrylic acid ionomers. Macromolecules. 2006;39(3):1079–1086.
58 Kumar UN, Kratz K, Behl M, et al. Shape-memory properties of magnetically active triple-shape nanocomposites based on a grafted polymer network with two crystallizable switching segments. Express Polym Lett. 2012;6(1):26–40.
59 Kratz K, Madbouly SA, Wagermaier W, et al. Temperature-memory polymer networks with crystallizable controlling units. Adv Mater. 2011;23(35):4058–4062.